Microscale Thermophysical Engineering, 9:63–84

ISSN: 1089-3954 print/1091-7640 online
DOI: 10.1080/10893950590913404

Taylor & Francis
Taylor & Francis Group

PHOTON LOCALIZATION AND ELECTROMAGNETIC FIELD ENHANCEMENT IN LASER-IRRADIATED, RANDOM POROUS MEDIA

X. L. Ruan and M. Kaviany
Department of Mechanical Engineering, University of Michigan, Ann Arbor, Michigan, USA

By solving Maxwell's equations, we observed photon localization and strong electromagnetic field enhancement in laser-irradiated, one-dimensional random multilayer and two-dimensional random media, with particle size around the laser wavelength. Higher refractive index contrast and degree of randomness result in stronger localization. The probability density and the location of enhanced fields are investigated as functions of refractive index and particle size distribution. For weakly dissipative media, local absorption enhancement is observed, and the expectation intensity distribution is obtained by averaging among many realizations. For comparison, the equation of radiative transfer (ERT) is also solved for random porous media, using the two-flux model. Since no interference effects are allowed, the classical diffusion, rather than localization, is predicted. Consequently, ERT can represent a good statistical average of the intensities only as absorption is dominant over localization. As expected, the particle treatment of ERT does not allow for predicting photon localization and field enhancement.

Radiative transport in random porous media has long been an important problem in science and engineering [1–3]. As a laser beam is irradiated on a nonabsorbing random porous medium in which the particle size is much larger than the laser wavelength, the transmissivity reveals a diffusive behavior; i.e., decays inversely with the medium thickness [4]. Recently, however, it has been found that as the particle size decreases to the order of the laser wavelength, the diffusion breaks down and the transmission coefficient decays exponentially with the medium thickness, due to the constructive interference among the multiply scattered waves [5, 6]. This phenomenon, termed "photon localization," is the counterpart of electron localization suggested by Anderson [7] and has been investigated theoretically and experimentally in one- [8–13], two- [14–20], and three- [21–24] dimensional structures. With the onset of localization, the electromagnetic (EM) waves may not propagate through, but are confined in a finite spatial region, forming a "random resonator." This property has initiated intense research interest in random lasers

Received 6 November 2003; accepted 30 November 2004.
The collaboration and assistance of Professor Steven Rand and Dr. Shawn Redmond of the Department of Electrical Engineering and Computer Science and the Applied Physics Program at the University of Michigan, and the comments by Professor Zhuoming Zhang of Georgia Institute of Technology, are greatly appreciated.
Address correspondence to M. Kaviany, Department of Mechanical Engineering, University of Michigan, Ann Arbor, MI 48109-2125. E-mail: kaviany@umich.edu

NOMENCLATURE

d_s	solid particle size, nm
E	complex electric field, V/m
f	probability density
$\mathbf{H}$	magnetic field vector, A/m
I	intensity, W/m^2
k	wave number, m^{-1}
l_{loc}	localization length
l_m	mean free path
L	length of the porous medium, m
m	complex refractive index
n	refractive index
p	probability
$\mathbf{S}$	Poynting vector, W/m^2
$\dot{s}$	volumetric energy generation rate, W/m^3
T	transmissivity
W	bin width
x	coordinate, m

Greek Symbols

δ	delta function
ε	porosity, dielectric constant
ε_0	free space electric permittivity, F/m
θ	scattering angle
κ	extinction index
λ	wavelength, nm
μ_0	free space permeability, H/m
σ	electric conductivity, S/m
σ_a	absorption coefficient, 1/m
σ_{ex}	extinction coefficient, 1/m
σ_s	scattering coefficient, 1/m
Φ	scattering phase function
ω	angular frequency, 1/s

Subscript

a	absorption
ex	extinction
f	fluid
i	incident
r	reflected
s	solid, scattering
t	transmitted

Superscript

*	dimensionless quantity
+	forward
−	backward

[25–33], in which the "random resonator" may replace the resonator in conventional lasers and remarkably simplify the device.

The interference effects on the radiative transport must be properly addressed in order to understand photon localization. This can be done using the direct simulation in which Maxwell's equations are solved for the porous medium, and the boundary conditions are matched at the interfaces between particles and pores. Because the geometries of the interfaces are generally complicated, the direct simulation is computationally expensive, except for simple geometries. For example, it has been performed using the transfer matrix method for one-dimensional multilayer [8], and using the FDTD (finite-difference time domain) or the transfer matrix method [14, 15] for simple two-dimensional random systems. Photon localization is predicted in both dimensions by showing that the calculated transmissivities decay exponentially with the medium thickness. However, this "transmission" approach does not show explicitly the role played by interference in the onset of localization. Recently, local field amplitudes, rather than transmissivities, have been calculated for one-dimensional random media, and the internal field is found to be orders higher than the incident field [34]. This large field enhancement is exactly a signature of interference and has many implications.

Traditionally, the effective medium approximations have been used to treat the radiative transport in random porous media, because the direct simulation mentioned above is usually computationally too heavy to be practical. The equation of radiative transfer (ERT) is the most widely used effective medium treatment [35]. The scattering and absorption properties are derived from the spectral radiative behavior of a single isolated

particle (Mie scattering) using large and small particle size approximations. The effective properties are then obtained based on the porosity and particle size distribution. Inclusions of the interparticle interactions (dependent scattering) have also been made [2]. The ERT is then solved using some approximations (e.g., two-flux approximation) to obtain the local radiative intensity. The Maxwell–Garnett approximation is another effective medium approximation for the determination of the effective, bulk dielectric properties of inhomogeneous materials [36]. In this approach the field induced in a uniform host by a single spherical or ellipsoidal inclusion is calculated exactly, and the field's distortion by the electrostatic interaction between the inclusions is treated approximately [37]. The effective permittivity is then obtained, and Maxwell's equations are solved for the local radiative intensity. Because the effective medium approximations require the use of effective properties obtained by volumetric averaging, they do not allow for coherent interference effects and are not expected to predict photon localization and field enhancement.

Here, by solving Maxwell's equations (EM theory), the transmissivity of a one-dimensional random multilayer is studied as a function of the sample thickness, and through its exponential decay the photon localization is observed. The effects of the refractive index contrast and the degree of randomness on localization length are investigated, too. To show the role played by interference in the onset of localization, the local electromagnetic field is determined for one- and two-dimensional random media, using the transfer matrix method and a code based on finite element method (HFSS), respectively. The results show field enhancement of a few orders of magnitude higher than the incidence in some realizations. Based on the results predicted by EM theory, an electromagnetic statistical (EMS) approach is proposed where the intensity distributions of a sufficient number of realizations are averaged to obtain the expectation intensity distribution. For comparison, the radiative transfer in random porous media is also treated with the effective medium approximations (here ERT). The transmissivity decays inversely with the sample thickness and thus manifests a diffusion behavior, rather than the localization behavior predicted by EM theory. For this reason, it is found that the intensity distribution predicted by ERT can agree with that by EMS only in absorption-dominated media. The existing effective medium approximations (ERT and EMS) are not capable of predicting the local field enhancement and photon localization.

PHOTON LOCALIZATION

The simplest structure to study photon localization is the one-dimensional random multilayer system, as shown in Figure 1. It has a finite length L in the direction of the electromagnetic wave propagation x, and an infinite length in the plane normal to x. It can thus be treated as a one-dimensional system. The dielectric solid material has a complex refractive index m_s $(= n_s - i\kappa_s)$, while the fluid is assumed to be air and has the refractive index m_f $(= n_f = 1)$.

The transfer matrix method [38, 39] is used to solve Maxwell's equations in this multilayer medium, subject to a uniform normal incident field E_i. The field in the medium can be divided into two components, the forward (transmitted) component E^+ and the backward (reflected) component E^-, also shown in Figure 1. At the interface of two different media with the refractive indices m_s and m_f, these components are related by

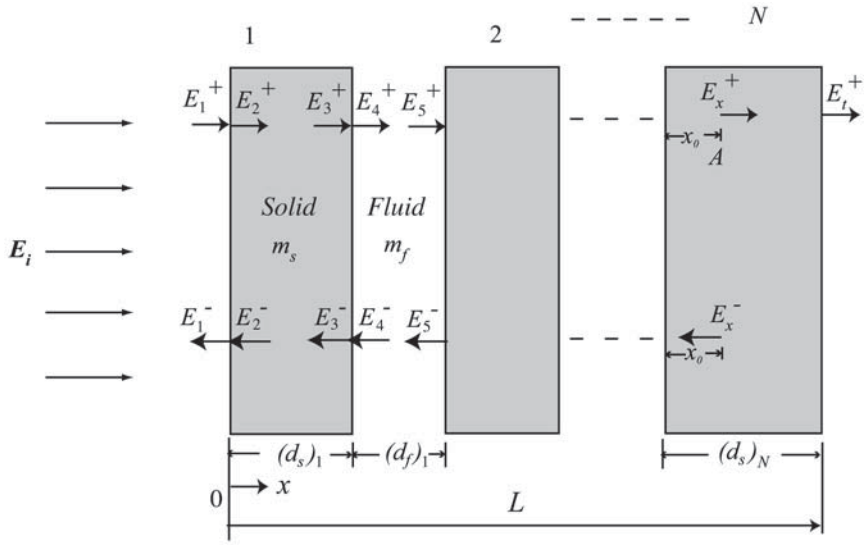

Figure 1. Parallel solid layers with random thicknesses (one-dimensional random multilayer). The fluid layer thickness is also random. The average porosity is prescribed.

the transfer matrix:

$$\begin{bmatrix} E_1^+ \\ E_1^- \end{bmatrix} = \begin{bmatrix} \dfrac{m_s + m_f}{2m_f} & \dfrac{m_s - m_f}{2m_f} \\ \dfrac{m_s - m_f}{2m_f} & \dfrac{m_s + m_f}{2m_f} \end{bmatrix} \begin{bmatrix} E_2^+ \\ E_2^- \end{bmatrix} \tag{1}$$

The components within a given layer are related by the transfer matrix

$$\begin{bmatrix} E_2^+ \\ E_2^- \end{bmatrix} = \begin{bmatrix} e^{ik_s(d_s)_1} & 0 \\ 0 & e^{-ik_s(d_s)_1} \end{bmatrix} \begin{bmatrix} E_3^+ \\ E_3^- \end{bmatrix} \tag{2}$$

where k_s $(= 2\pi m_s/\lambda_0)$ is the wave number and λ_0 is the wavelength in vacuum. Equations (1) and (2) are repeated for all layers. If tracing all N layers, the fields at the first and the last boundaries are related through

$$\begin{bmatrix} E_1^+ \\ E_1^- \end{bmatrix} = \left[\prod_{j=1}^{N-1} (M_{s,j} M_{f,j}) \right] M_{s,N} \begin{bmatrix} \dfrac{m_f + m_s}{2m_s} & \dfrac{m_f - m_s}{2m_s} \\ \dfrac{m_f - m_s}{2m_s} & \dfrac{m_f + m_s}{2m_s} \end{bmatrix} \begin{bmatrix} E_t^+ \\ 0 \end{bmatrix} \tag{3}$$

where

$$M_{s,j} = \begin{bmatrix} \dfrac{m_s + m_f}{2m_f} & \dfrac{m_s - m_f}{2m_f} \\ \dfrac{m_s - m_f}{2m_f} & \dfrac{m_s + m_f}{2m_f} \end{bmatrix} \begin{bmatrix} e^{ik_s(d_s)_j} & 0 \\ 0 & e^{-ik_s(d_s)_j} \end{bmatrix} \tag{4}$$

and

$$M_{f,j} = \begin{bmatrix} \dfrac{m_f + m_s}{2m_s} & \dfrac{m_f - m_s}{2m_s} \\ \dfrac{m_f - m_s}{2m_s} & \dfrac{m_f + m_s}{2m_s} \end{bmatrix} \begin{bmatrix} e^{ik_f(d_f)_j} & 0 \\ 0 & e^{-ik_f(d_f)_j} \end{bmatrix} \tag{5}$$

Given the incident field E_1^+ $(= E_i)$, the reflected field E_1^- $(= E_r)$ and the transmitted field E_t^+ are found from Eq. (3). The transmissvity T is then given by

$$T = \left| \frac{E_t^+}{E_i} \right|^2 \tag{6}$$

We calculated the transmissivity for a model multilayer with 50 layers in which the layer thicknesses d_s follow a uniform distribution between $\langle d_s \rangle \pm \Delta d_s = 1000 \pm 800$ nm, and with the porosity $\varepsilon = 0.35$, $n_s = 1.8$, and $\kappa_s = 0$ (n_s and κ_s are for doped yttria compacts off-resonance [40]). To generate such a multilayer, we have an infinite number of possibilities, each of which is called a "realization." The nonabsorbing material is used to remove the possibility of causing exponential decay by absorption. To investigate the transmissivity as a function of the sample thickness, we add one layer to the sample at one time and thus obtain a series of transmissivities. The dots shown in Figure 2 represent these transmissivities for one typical realization when there are $1, 2, \ldots, 50$ layers. These dots are fitted well using an exponential decay line, indicating that localization takes place. The localization length of this realization can be obtained from the slope of the fitted line

$$l_{\text{loc}} = -\frac{dL}{d(\ln T)} \tag{7}$$

There are infinite possible realizations for this model multilayer, and localization behavior is observed in all realizations that we have tried. This supports the statement that random systems in one-dimensional always exhibit localization [8]. The localization length of

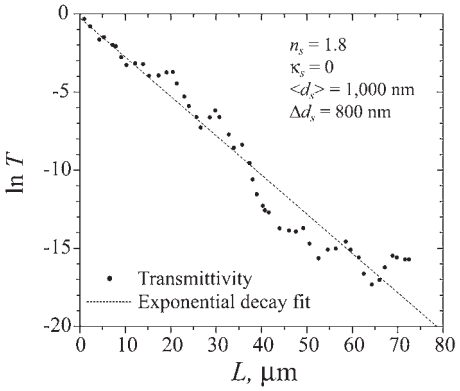

Figure 2. Variation of the transmissivity as a function of the medium thickness. The dots are the transmissivities obtained by adding layers to the medium, one at a time, and the dashed line is an exponential decay fit.

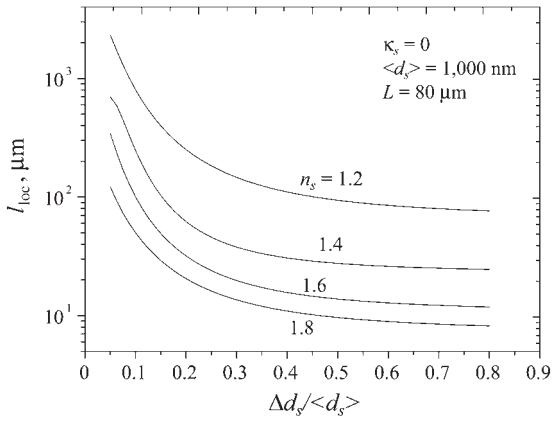

Figure 3. Effects of the refractive index contrast and the degree of randomness on the localization length.

this model multilayer is obtained by averaging the localization lengths of numerous realizations.

The effects of the refractive index contrast and the degree of randomness on localization length are investigated, and the results are shown in Figure 3. As expected, higher refractive index contrast and higher degree of randomness cause smaller localization lengths or stronger localization.

FIELD ENHANCEMENT

The results in the previous section have confirmed the occurrence of photon localization. But what causes localization remained confusing for some time. Now it is commonly believed to be due to the constructive interference among the multiply scattered waves. However, the transmissivity profile in Figure 2 does not show any explicit signature of interference. Recently, the local field amplitude, rather than the transmissivity, was investigated for random multilayer, and strong field enhancement was observed [34]. This provides an exact signature of strong, constructive wave interference.

One-Dimensional Multilayer

Let's follow the solution procedure developed in the last section for multilayer system. Once E_1^- is determined, the local electric field can be determined for any point (in practice, a large number of points) in the medium. For an arbitrary site A, which lies in the Mth layer, at a distance x_0 from the layer surface and x from the medium surface (Figure 1), the field is related to that at the first interface by

$$\begin{bmatrix} E_1^+ \\ E_1^- \end{bmatrix} = \left[\prod_{j=1}^{M-1} (M_{s,j} M_{f,j}) \right] \begin{bmatrix} \dfrac{m_s + m_f}{2m_f} & \dfrac{m_s - m_f}{2m_f} \\ \dfrac{m_s - m_f}{2m_f} & \dfrac{m_s + m_f}{2m_f} \end{bmatrix} \begin{bmatrix} e^{ik_s x_0} & 0 \\ 0 & e^{-ik_s x_0} \end{bmatrix} \begin{bmatrix} E_x^+ \\ E_x^- \end{bmatrix} \quad (8)$$

The magnitude of the local field is then given by

$$|E(x)| = |E_x^+ + E_x^-| \tag{9}$$

The local electric field is determined in a similar model multilayer with 50 layers and is subject to a same irradiation as in the previous section. There are infinite possible realizations for this model multilayer, and the field results for one of them are shown in Figure 4(a), where the dimensionless electric field is defined as $|E|^* = |E|/|E_i|$.

From Figure 4(a) it is evident that there is field enhancement; i.e., there are peaks in the field inside the medium that can be a few orders of magnitude larger than the incident field for this realization. Thus, the energy density of the electric field can be two or even more orders of magnitude larger than the incident value. In periodic multilayer, the electric field is also periodic, resulting in no isolated peaks inside the media (even if the field in this case can also be higher than the incident field). The physical basis

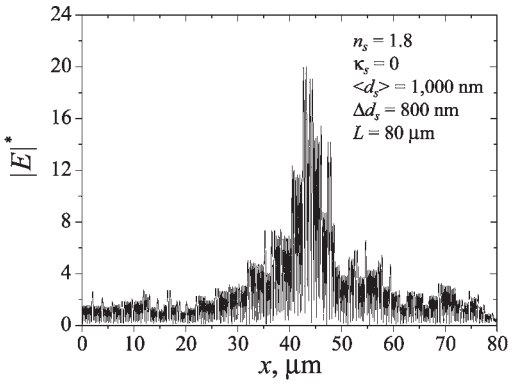

(a)

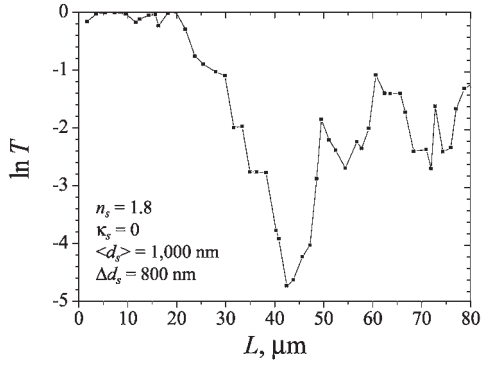

(b)

Figure 4. (a) Local field distribution in a random multilayer with field enhancement shown. (b) Variation of the transmissivity as a function of the medium thickness in the same multilayer.

of field enhancement is electromagnetic wave interference. In the random multilayer system, the waves will multiply, transmit, and reflect at all interfaces and interfere with each other. At some sites for some realizations, the interference is so ideally constructive that it results in an extremely large field. Thus, the large field enhancement is directly attributed to randomness and cannot be observed in homogeneous or periodic media. Note that the coherence condition that the medium size is smaller than the coherence length must be satisfied to observe the field enhancement. The coherence length is $\lambda^2/\Delta\lambda$ for a central wavelength λ and a spectrum width $\Delta\lambda$ [41]. In this study we assume a monochromatic wave, thus satisfying the coherence condition ($\Delta\lambda$ is 0 and the coherence length is infinite). The coherence length of many lasers is several kilometers, satisfying the coherence condition.

It's interesting to see how the transmissivity evolves layer by layer in such a realization that allows field enhancement. This is shown in Figure 4(b). Different from the situation in Figure 2, in which the transmissivity reveals a good exponential decay behavior, the variation of transmissivity with sample thickness in Figure 4(b) has a large fluctuation, but localization is still considered to happen, since diffusion obviously breaks down. It is anti-intuitional that just after field enhancement is onset, there is a region in which the transmissivity increases, rather than decreases, with the sample thickness. Also, the final transmissivity is much larger than that in Figure 2. However, it is natural to understand this by recognizing that more photons have to travel through and interfere with each other to establish a large local field. Although realizations allowing field enhancement generally have larger transmissivity, the field is more trapped in a wavelength sized region, forming a "random resonator." This property is very attractive to laser science since it may replace the resonator in conventional lasers. Experimentally, laser actions in random gain media have been observed [26].

Two-Dimensional Geometry

The two-dimensional random porous medium used in this study is shown sketchily in Figure 5(a). The solids are arranged as an array of infinitely long (in the y direction) dielectric cylinders with random radii and locations. We again examine the wave propagation subject to incidence of a planar electromagnetic wave upon this structure, traveling in the x-direction. Maxwell's equations in two-dimensional random media have been solved using FDTD or the transfer matrix method [14,15], but the degree of randomness has been limited by the mesh size, and thus the media could not be systematically randomized. In this study, the cylinder size radii and locations are entirely random (the only limitation is that the cylinders should not overlap). A code based on the finite element method, high-frequency structure simulator (HFSS), is used [22]. A finite computation domain is chosen, resulting in six surfaces or boundaries. The two x-z boundaries are taken as being periodic to simulate the infinite length in the y direction. The two x-y boundaries are also taken as being periodic. The y-z planes are set to be the incident boundary at $x = 0$ and the radiation boundary at $x = L$.

We choose a computation domain of $5 \times 1 \times 5\ \mu\text{m}^3$. Again, the local electric field in this region is determined for a normal incident electromagnetic wave of wavelength $\lambda = 1000$ nm for a two-dimensional random medium composed of 20 long cylinders with a random diameter between $\langle d_s \rangle \pm \Delta d_s = 1000 \pm 400$ nm, and with $n_s = 1.8$ and $\kappa_s = 0$ in air. The results are shown in Figure 5(b), using contours of constant dimensionless

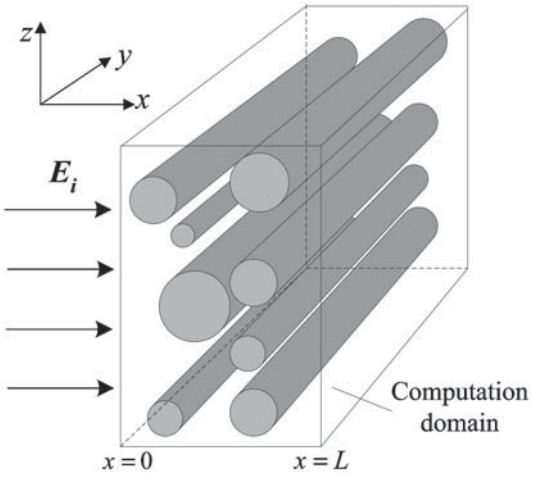

(a)

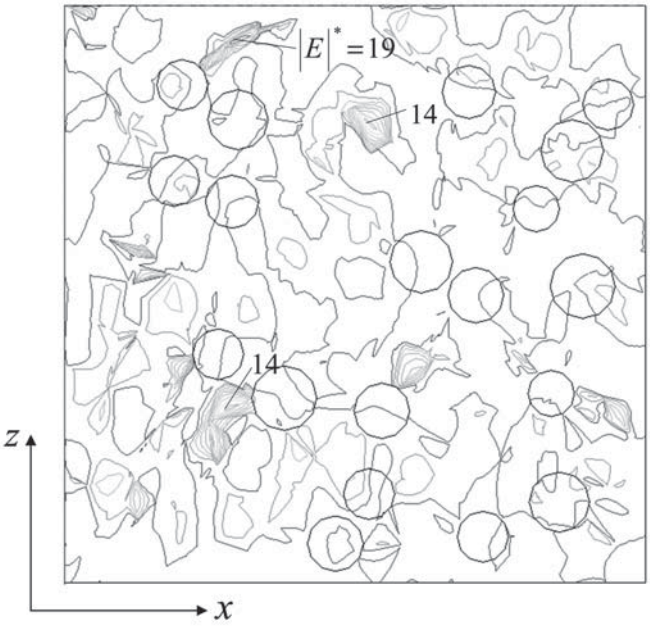

(b)

Figure 5. (a) The two-dimensional geometry composed of infinitely long cylinders. (b) The two-dimensional distribution of the dimensionless field magnitude $|E|^*$ for a realization; the circles are the sections of the cylinders. The porosity is 0.85.

electric field. Similar to the one-dimensional case, there are sites of field enhancement within the random porous medium that can be a few orders higher of magnitude than the incident field.

Factors that Influence Occurrence of Field Enhancement

The electric field distributions described above are examples of individual realizations with large field enhancements. Determining the structural characteristics related to the maximum field enhancement is not attempted. However, statistical averaging over numerous realizations can help in understanding the conditions under which large field enhancements are more probable. For the one-dimensional multilayer, we compute $N_t = 192 \times 10^5$ local field values $|E|^*$, from $N_r = 6{,}000$ different realizations, each of which gives $N_n = 3{,}200$ field values. From these, we compute the probability density function $f(|E|^*)$. This is found by first dividing all of the field values (from 0 to $|E|^*_{\max}$) into a number of (say, N_b) bins (intervals) and then determining the number of field values in each bin. Finally the probability density f_i for the ith bin is found from

$$f_i = \frac{M_i}{N_t W_b} = \frac{M_i N_b}{N_t |E|^*_{\max}} \tag{10}$$

where M_i is the number of occurrences in the ith bin and $W_b = |E|^*_{\max}/N_b$ is the bin width. In our 6,000 realizations, $|E|^*_{\max}$ is 20.1.

The results are shown in Figures 6(a) to (d) for several values of the refractive index (n_s, κ_s), average layer size ($\langle d_s \rangle/\lambda$), and the degree of randomness ($\Delta d_s/\langle d_s \rangle$). As shown in Figures 6(a), (b), and (d), the higher the values of n_s, κ_s, and $\Delta d_s/\langle d_s \rangle$, the higher the probability of an occurrence of small $|E|^*$; i.e., there is less probability for field enhancement ($|E|^* > 1$). At the same time, as indicated in Figures 6(a) and (d), the higher the values of n_s and $\Delta d_s/\langle d_s \rangle$, the higher the probability of occurrence of large field enhancement. As shown in Figure 6(c), the average size parameter does not affect the field significantly. It should be noted that $|E|^*_{\max}$ is not shown here because of its extremely small probability.

The locations of the field enhancement are determined using the same samplings mentioned above; i.e., the $N_r = 6{,}000$ realizations, each of which gives $N_n = 3{,}200$ field values at the same set of 3,200 sampling locations. Then for every site x, there are N_r different field values $|E|^*$, some of which (say, N_e) are enhanced ($|E|^* > 1$). The probability $p(x)$ of having field enhancement ($|E|^* > 1$) at a site x is found by dividing the number of the occurrences of field enhancement N_e by N_r. This probability is plotted for each of the 3,200 sites, as shown in Figure 7. The field at sites closer to the incident surface is always more probable to be enhanced. Also, the higher the values of n_s, κ_s, $\langle d_s \rangle/\lambda$, and $\Delta d_s/\langle d_s \rangle$, the less is the probability of field enhancement.

ABSORPTION ENHANCEMENT IN DISSIPATIVE MEDIA

Nonabsorbing medium is used to investigate localization as described previously to show that the exponential decay of transmissivity is caused indeed by recurrent scattering, rather than absorption. However, real media always have some absorption. It has been shown that photon localization still happens in weakly dissipative media [8].

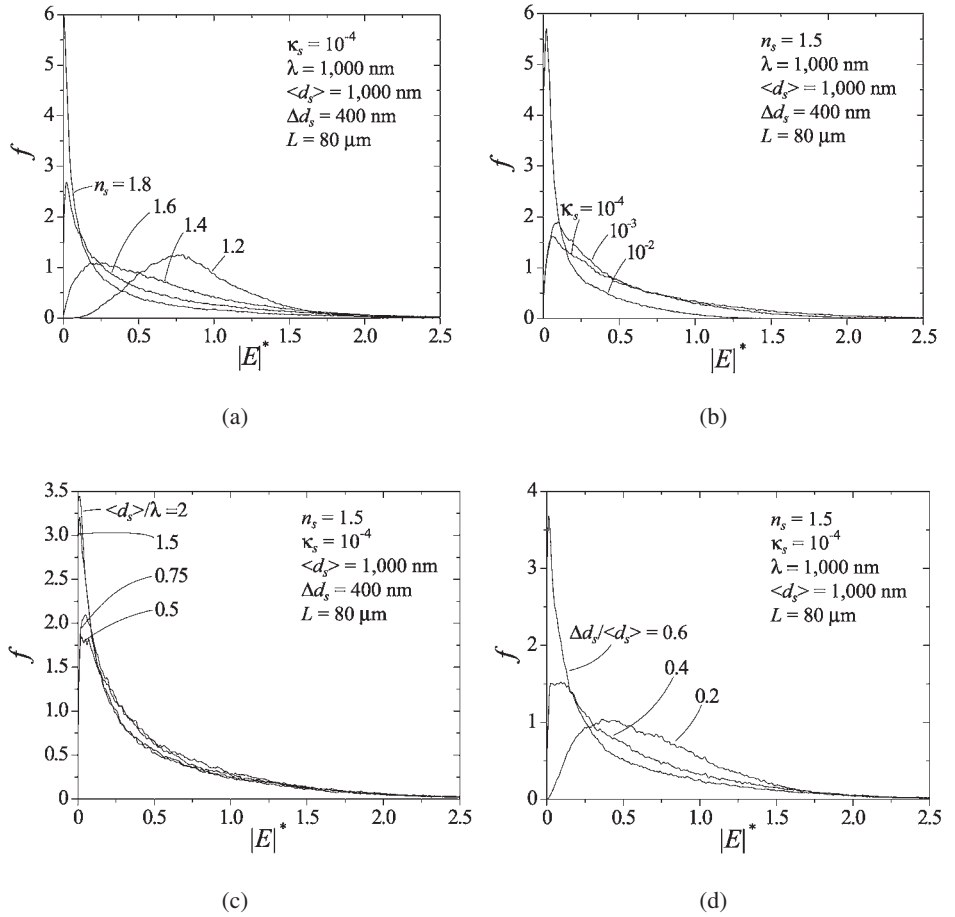

Figure 6. Probability density function for $|E|^*$ within a random porous medium, showing the effects of solid (a) refractive index, (b) extinction index, (c) size parameter, and (d) size distribution. The porosity is 0.35.

In this section, our interest is put on the local absorption and heat generation in the medium.

Again consider the multilayer in Figure 1, the local intensity is given by the time average of the Poynting vector **S** as

$$I(x) = |\bar{\mathbf{S}}| = \frac{1}{2}|\mathrm{Re}[\mathbf{E}(x) \times \mathbf{H}^*(x)]| \tag{11}$$

where $\mathbf{H}(x)$ is the magnetic field. According to the energy conservation law, the power loss per unit volume (or the volumetric heat generation rate) $\dot{s}$ is defined by the spatial decay rate of the intensity

$$\dot{s} = -\frac{dI}{dx} \tag{12}$$

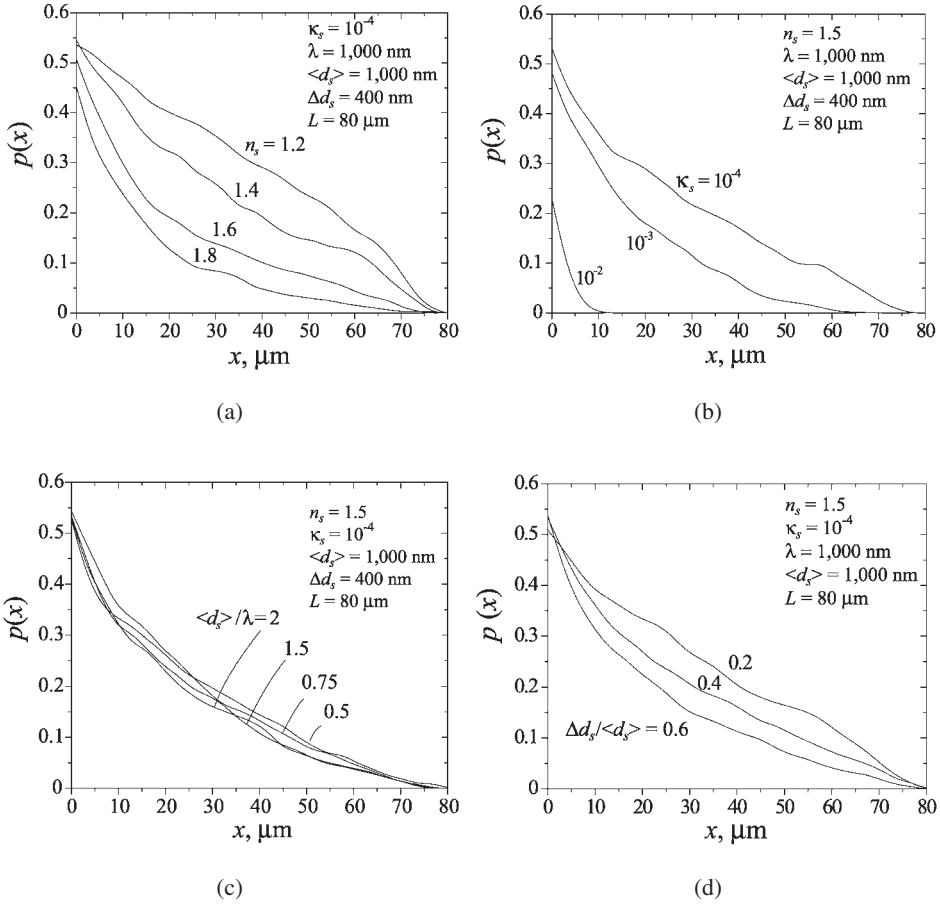

Figure 7. Probability of field enhancement as a function of locations. Effects of solid (a) refraction index, (b) extinction index, (c) size parameter, and (d) size distribution. The porosity is 0.35.

and the extinction coefficient σ_{ex} is defined as the ratio of heat generation rate $\dot{s}$ to the local intensity I

$$\sigma_{\text{ex}} = \frac{\dot{s}}{I} = -\frac{1}{I}\frac{dI}{dx} \tag{13}$$

From electromagnetic wave theory, the power loss per unit volume for this lossy dielectric medium is [43]

$$\dot{s} = \frac{1}{2}\sigma|E|^2 = \frac{1}{2}\omega\varepsilon''|E|^2 \tag{14}$$

where σ is the electric conductivity, ω is the angular frequency, and ε'' is the imaginary part of the dielectric constant ε, which is related to the complex refractive index m through

$$\varepsilon = \varepsilon' - i\varepsilon'' = \varepsilon_0 m^2 \tag{15}$$

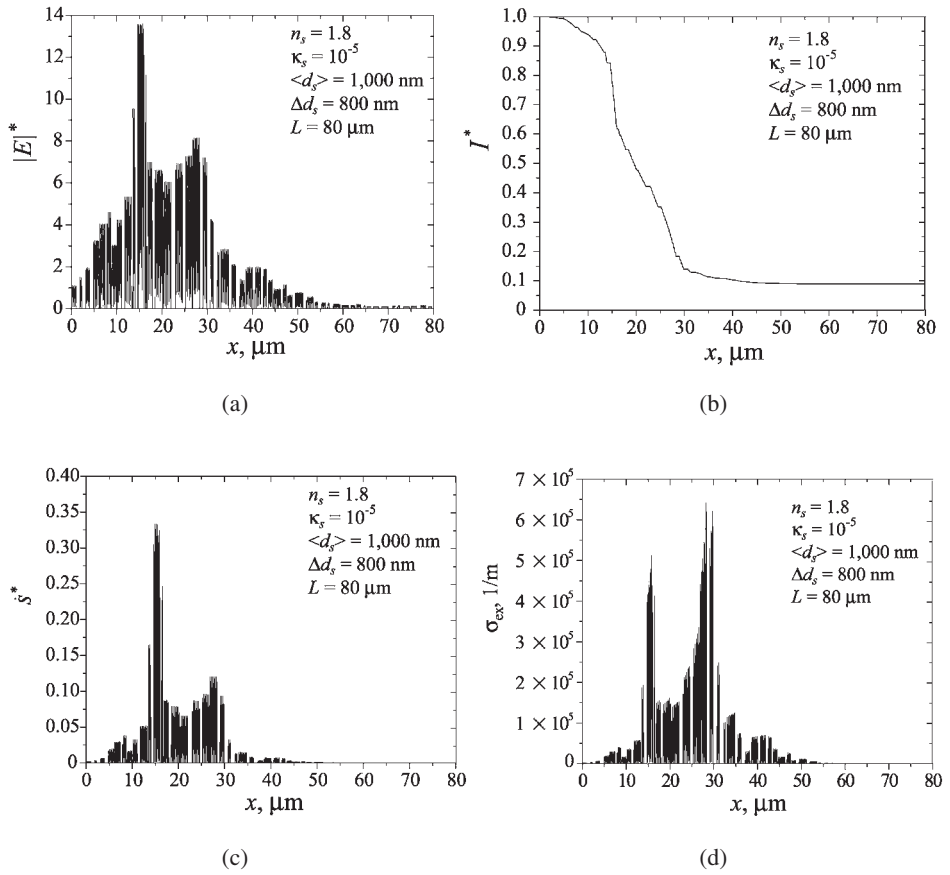

Figure 8. Distributions of the dimensionless (a) electric field, (b) intensity, (c) volumetric heat generation rate, and (d) extinction coefficient, for a weakly absorbing multilayer. The porosity is 0.35.

where ε_0 is the free-space permittivity. Then Eq. (14) becomes:

$$\dot{s} = \frac{2\pi n \kappa_s}{\lambda_0} \sqrt{\frac{\varepsilon_0}{\mu_0}} |E|^2 \tag{16}$$

where μ_0 is the free space permeability. Equations (12) and (16) give the same result, but Eq. (16) shows that $\dot{s}$ is explicitly proportional to the square of the electric field.

The local electric field is again determined subject to a normal incident electromagnetic wave of wavelength $\lambda = 1{,}000$ nm in a one-dimensional random multilayer with 50 solid layers whose thicknesses d_s follow a uniform distribution between $\langle d_s \rangle \pm \Delta d_s = 1000 \pm 800$ nm, and with the porosity $\varepsilon = 0.35$, $n_s = 1.8$, and $\kappa_s = 10^{-5}$ (n_s and κ_s are for doped yttria compacts on resonance [40]). There are infinite possible realizations for this model composite, and the field results for one of them are shown in Figures 8(a) to (d), where the dimensionless parameters are defined as, $|E|^* = |E|/|E_i|$, $I^* = I/I_i$, and $\dot{s}^* = \dot{s}\langle d_s \rangle / I_i$.

From Figure 8(a) it is evident that field enhancement is still possible in weakly absorbing multilayer system, suggesting that scattering is dominant over absorption. The distribution of the intensity, which decays with a random rate, is shown in Figure 8(b). As shown in Figure 8(c), the volumetric heat generation rate $\dot{s}$ due to absorption has a similar distribution as that of the electric field, because $\dot{s}$ is proportional to the square of the field, according to Eq. (16). The peak of $\dot{s}$ inside the medium indicates that a local melting may happen at that site. The distribution of the local extinction coefficient σ_{ex} is presented in Figure 8(d). The maximum of σ_{ex} does not necessarily coincide with the maximum of $\dot{s}$, because σ_{ex} is the ratio of $\dot{s}$ and the local intensity.

ELECTROMAGNETIC STATISTICAL (EMS) APPROACH

For a given particle mean size and porosity, and a spread in the particle size, infinite realizations of one-dimensional random multilayer (and associated filed distributions) are possible. The probability for occurrence of a given realization is rather low, but the statistical average of the intensity distributions of a sufficient number of realizations represents the intensity expectation distribution in the medium reasonably. This approach, here called the electromagnetic statistical (EMS) approach, is explained in Figure 9. A model multilayer with 250 layers is considered, and 6,000 realizations are used. Note that we use a longer sample than before, in order to show more effectively the variation of local intensity with location. For each realization, we calculate the local intensity using the same method developed in the previous section, and record the intensity values at 3,200 sampling sites. Then, for each of the 3,200 sites, we determine its expectation intensity by averaging the field values of that site of 6,000 realizations. To be clearer, the results of only two (compared to 3,200) typical realizations, each of which is calculated similarly with the intensity distribution in Figure 8(b), are shown in Figure 9. The results are presented in Figure 10 for weakly and strongly absorbing materials, respectively. The expectation intensities decay exponentially in the direction of wave propagation.

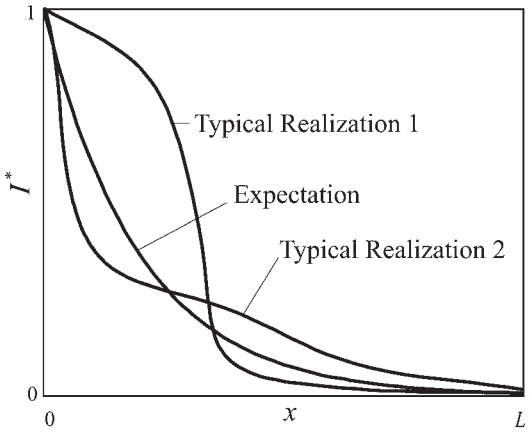

Figure 9. Distributions of dimensionless intensities for two typical realizations. The expectation intensity is determined among the realizations.

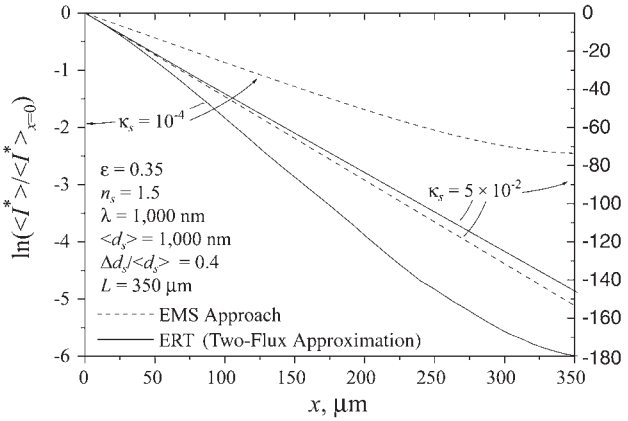

Figure 10. Comparison of the intensity distributions obtained by the EMS and ERT for a one-dimensional multilayer porous medium, as $\kappa_s = 10^{-4}$ and $\kappa_s = 5 \times 10^{-2}$, respectively.

PREDICTIONS OF EQUATION OF RADIATIVE TRANSFER (ERT)

Formulation and Solution Procedure

The radiation transport within the same composite described in previous sections can also be treated using the ERT. In this treatment, the scattering properties of a single particle are derived first, using small and large particle size approximations. The effective scattering properties are then determined for a cluster of particles, based on the porosity and particle size distribution. Finally, the ERT is solved using proper approximations, such as the two-flux model.

For a one-dimensional multilayer system, a layer serves as a single scatterer. For the normal incidence of a planar radiation upon a planar particle, as shown in Figure 11, the scattering is by reflection. Using the transfer matrix method, the incident, transmitted and reflected fields are related through

$$\begin{bmatrix} E_i \\ E_r \end{bmatrix} = \begin{bmatrix} \dfrac{m_s + m_f}{2m_f} & \dfrac{m_s - m_f}{2m_f} \\ \dfrac{m_s - m_f}{2m_f} & \dfrac{m_s + m_f}{2m_f} \end{bmatrix} \begin{bmatrix} e^{ik_s d_s} & 0 \\ 0 & e^{-ik_s d_s} \end{bmatrix} \cdot \begin{bmatrix} \dfrac{m_f + m_s}{2m_s} & \dfrac{M_f - m_s}{2m_s} \\ \dfrac{m_f - m_s}{2m_s} & \dfrac{m_f + m_s}{2m_s} \end{bmatrix} \begin{bmatrix} E_t \\ 0 \end{bmatrix} \tag{17}$$

Thus, E_r and E_t are derived in terms of E_i, and the transmission coefficient is a function of the layer thickness d_s, for a given m_f and m_s; i.e.,

$$T_r(d_s) = \frac{I_t}{I_i} = \frac{|E_t|^2}{|E_i|^2} \tag{18}$$

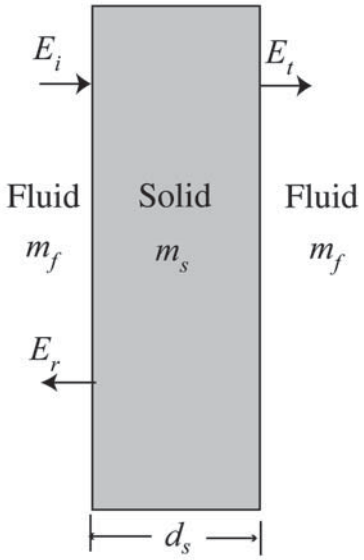

Figure 11. Transmission and reflection in a single solid layer.

The extinction coefficient of the single particle is defined as

$$\sigma_{\text{ex}}(d_s) = \frac{-\ln T_r(d_s)}{d_s} \tag{19}$$

For a random multilayer medium with porosity ε, where the layer thickness d_s follows a uniform distribution in the range of $\langle d_s \rangle \pm \Delta d_s$, the effective extinction coefficient becomes

$$\langle \sigma_{\text{ex}} \rangle = \frac{\int_{\langle d_s \rangle - \Delta d_s}^{\langle d_s \rangle + \Delta d_s} -\ln T_r(d_s) \mathrm{d}d_s}{\int_{\langle d_s \rangle - \Delta d_s}^{\langle d_s \rangle + \Delta d_s} d_s \mathrm{d}d_s} (1 - \varepsilon) \tag{20}$$

The effective absorption coefficient is

$$\langle \sigma_a \rangle = \frac{4\pi \kappa_s}{\lambda_0} (1 - \varepsilon) \tag{21}$$

The effective scattering coefficient is found from

$$\langle \sigma_s \rangle = \langle \sigma_{\text{ex}} \rangle - \langle \sigma_a \rangle \tag{22}$$

Since scattering occurs only in the backward direction, the scattering phase function is a delta function; i.e.,

$$\Phi(\theta) = \delta(\theta - \pi), \int_{-1}^{1} \Phi(\theta) \mathrm{d}\ \cos\theta = 2 \tag{23}$$

Then the ERT becomes [35]

$$\cos\theta\frac{dI(x,\theta)}{dx} = -(\langle\sigma_s\rangle + \langle\sigma_a\rangle)I(x,\theta) + \frac{\langle\sigma_s\rangle}{2} \cdot \left[\int_0^1 I(x,\theta_i)\Phi(\theta_i-\theta)\mathrm{d}\ \cos\theta_i + \int_{-1}^0 I(x,\theta_i)\Phi(\theta_i-\theta)\mathrm{d}\ \cos\theta_i\right] \tag{24}$$

For a normal irradiation on a one-dimensional geometry, the radiative intensity has only two components; namely, forward and backward. Thus, the two-flux approximation can be used to solve Eq. (24). By taking $\theta = 0$ and defining $I(x,0) = I^+$ and $I(x,\pi) = I^-$, Eq. (24) gives for the forward intensity

$$\frac{dI^+}{dx} = -(\langle\sigma_s\rangle + \langle\sigma_a\rangle)I^+ + \langle\sigma_s\rangle[(1-B)I^+ + BI^-] \tag{25}$$

where

$$B = \frac{1}{2}\int_{-1}^0 \Phi(\theta_i)\mathrm{d}\ \cos\theta_i = 1 \tag{26}$$

Equation (25) can then be simplified to

$$\frac{dI^+}{dx} = -(\langle\sigma_s\rangle + \langle\sigma_a\rangle)I^+ + \langle\sigma_s\rangle I^- \tag{27}$$

Similarly, by taking $\theta = \pi$, Eq. (24) gives for the backward intensity

$$-\frac{dI^-}{dx} = -(\langle\sigma_s\rangle + \langle\sigma_a\rangle)I^- + \langle\sigma_s\rangle I^+ \tag{28}$$

The boundary conditions for Eqs. (27) and (28) are

$$I^+(0) = 1,\ I^-(L) = 0 \tag{29}$$

Photon Diffusion in Nonabsorbing Random Media

Being an effective medium, particle-based transport equation, we expect ERT not to be capable of predicting photon localization. Again, a nonabsorbing medium is used to remove the possibility of causing exponential decay by absorption. Equations (25) and (26) are thus simplified to

$$\begin{cases} \dfrac{dI^+}{dx} = -\langle\sigma_s\rangle I^+ + \langle\sigma_s\rangle I^- \\ -\dfrac{dI^-}{dx} = -\langle\sigma_s\rangle I^- + \langle\sigma_s\rangle I^+ \end{cases} \tag{30}$$

The solution subject to boundary conditions given by Eq. (29) is

$$\begin{cases} I^+(x) = \dfrac{1 + \langle\sigma_s\rangle(L - x)}{1 + \langle\sigma_s\rangle L} \\ I^-(x) = \dfrac{\langle\sigma_s\rangle(L - x)}{1 + \langle\sigma_s\rangle L} \end{cases} \tag{31}$$

Then the transmissivity is found from

$$T(L) = I^+(L) = \frac{1}{1 + \langle\sigma_s\rangle L} \tag{32}$$

In random porous media, $\langle\sigma_s\rangle L$ is generally much larger than 1, and $T(L)$ has an inverse dependence on this; i.e., $T(L) = 1/[\langle\sigma_s\rangle L]$, which is characteristic of classical diffusion [21] with a mean free path $l_m = 1/\langle\sigma_s\rangle$. Thus, photon localization cannot be predicted by ERT, since the medium is averaged to obtain the effective scattering and absorption properties where wave interference effects are not allowed.

Absorption in Dissipative Random Media

For a dissipative medium, the solution of Eqs. (27) and (28) is

$$I^+(x) = \frac{(1 + \beta^2)\sinh[\gamma(L - x)] + 2\beta\cosh[\gamma(L - x)]}{(1 + \beta^2)\sinh(\gamma L) + 2\beta\cosh(\gamma L)} \tag{33}$$

$$I^-(x) = \frac{(1 - \beta^2)\sinh[\gamma(L - x)]}{(1 + \beta^2)\sinh(\gamma L) + 2\beta\cosh(\gamma L)} \tag{34}$$

where

$$\beta = [\langle\sigma_a\rangle/(\langle\sigma_a\rangle + 2\langle\sigma_s\rangle)]^{\frac{1}{2}} \tag{35}$$

and

$$\gamma = [\langle\sigma_a\rangle(\langle\sigma_a\rangle + 2\langle\sigma_s\rangle)]^{\frac{1}{2}} \tag{36}$$

The local intensity is the difference between the forward and backward intensities

$$I(x) = I^+(x) - I^-(x) \tag{37}$$

The predicted distributions of the normalized local intensity using ERT are shown in Figure 10 for $\kappa_s = 10^{-4}$ and 5×10^{-2}, respectively. The volumetric heat generation rate is

$$\dot{s}(x) = -\frac{dI(x)}{dx} \tag{38}$$

COMPARISON OF ERT, EMS, AND EM TREATMENTS: COMPETITION BETWEEN LOCALIZATION AND ABSORPTION

The intensity obtained using ERT are compared with the expectation values from the EMS (discussed previously). Both results decay exponentially, but with the same or different rates. This is determined by the nature of the two treatments. In the EMS treatment, the first step is to calculate the electric field exactly for each realization, where the detailed geometric features are kept and wave interference (dependent scattering) is allowed. The second step is to average the intensities among many realizations, where the dependent effect is still retained. In the ERT treatment, the first step is to average the medium to obtain the effective scattering and absorption properties, where the wave interference is not allowed. The second step is to calculate the intensity in this effective medium. Consequently, the results of ERT are for independent scattering and do not allow for photon localization. To quantitatively analyze this difference between the two treatments, we calculate the intensity decay (caused by both localization and absorption) for the two model composites, shown in Figure 10. The localization length is calculated in the absence of absorption using the method described previously, and the absorption length (penetration depth in EM theory) is calculated by $l_a = \lambda_0/[4\pi\kappa_s(1-\varepsilon)]$. For the weakly absorbing solid ($\kappa_s = 10^{-4}$), the localization and absorption lengths are 23.4 μm and 1224.3 μm, respectively, indicating that localization is dominant over absorption. The two treatments differ significantly since ERT does not allow for predicting localization. As the solid becomes more absorbing, the absorption becomes more important and localization becomes less important, and the two results are closer. For a highly absorbing material ($\kappa_s = 5 \times 10^{-2}$), the localization and absorption lengths are 23.4 μm and 2.4 μm, respectively, indicating that absorption is dominant over localization. The two treatments agree. This result indicates that although in both the ERT and EMS the intensity decays exponentially, the magnitudes do not generally agree, except for highly absorbing media. By introducing corrections to the scattering and absorption coefficients, based on the geometric and optical parameters, ERT may predict results similar to EMS. However, this scaling function must be complicatedly related to many parameters, such as the particle size distribution and the complex refractive index, and is not attempted here.

From the intensity profile (as shown in Figure 10), the extinction coefficients are determined for the EMS and ERT treatments using Eq. (13) and are compared to the extinction coefficient for one typical realization obtained using the EM theory. The results are shown in Figure 12. As can be seen, the effective medium approximations (EMS and ERT) give constant extinction coefficients through the medium, while the direct simulation (EM) theory gives spatially dependent extinction coefficients. At some sites, the local extinction coefficients can be up to a few orders higher of magnitude than the average extinction coefficients predicted by the effective medium approximations. Thus, only the direct simulation (EM theory) is capable of predicting the space-dependent enhanced absorption.

CONCLUSIONS

Electromagnetic wave interference plays a fundamental role in wave propagation and localization in random porous media. To allow for interference effects, a direct simulation (EM) has been used to solve the Maxwell's equations. Photon localization,

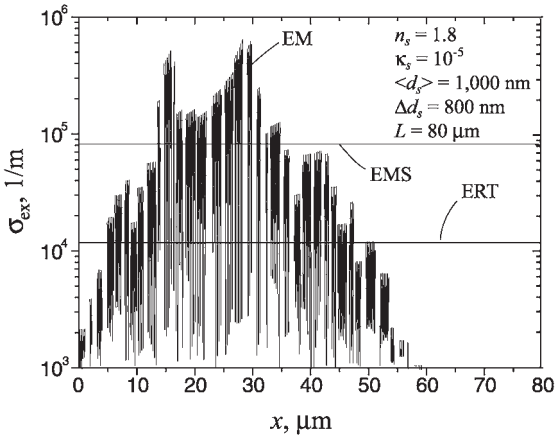

Figure 12. Comparison of the extinction coefficients predicted by EM, EMS, and ERT.

rather than the classical diffusion, is observed in a random multilayer. The local field calculations predict field enhancement up to a few orders of magnitude higher than the incident field. The field enhancement is caused by the ideally constructive interference at some sites for some realizations. The probability of enhanced $|E|^*$ and the locations of this enhancement are influenced by the solid complex refractive index and the particle size distribution. As a result of the spatially dependent, locally enhanced field, the spatially dependent absorption enhancement is also observed. Based on the EM theory, a new effective medium treatment, EMS, offers a reasonable distribution of the expectation intensity because it allows for the interference effects. In comparison, the traditional effective medium approximations (ERT here) require the use of effective properties obtained by volumetric averaging and do not directly allow for the interference effects. Consequently, they are unable to predict the strong, local field enhancement and photon localization.

REFERENCES

1. H. C. van de Hulst, Light Scattering by Small Particles, Dover Publications Inc., New York, 1981.
2. S. Kumar and C. L. Tien, Dependent Absorption and Extinction of Radiation by Small Particles, *Journal of Heat Transfer-Transactions of the ASME*, vol. 112, pp. 178–185, 1990.
3. M. I. Mishchenko, L. D. Travis, and A. A. Lacis, Scattering, Absorption, and Emission of Light by Small Particles, Cambridge University Press, New York, 2002.
4. P. Sheng, Introduction to Wave Scattering, Localization, and Mesoscopic Phenomena, Academic Press, San Diego, 1995.
5. D. Z. Zhang, W. Hu, Y. L. Zhang, Z. L. Li, B.Y. Cheng, and G. Z. Yang, Experimental Verification of Light Localization for Disordered Multilayers in the Visible-Infrared Spectrum, *Physical Review B*, vol. 50, pp. 9810–9814, 1994.
6. D. S. Wiersma, P. Bartolini, A. Lagendijk, and R. Righint, Localization of Light in a Disordered Medium, *Nature*, vol. 390, pp. 671–673, 1997.

7. P. W. Anderson, Absence of Diffusion in Certain Random Lattices, *Physical Review*, vol. 109, pp. 1492–1505, 1958.
8. A. R. McGurn, K. T. Christensen, F. M. Mueller, and A. A. Maradudin, Anderson Localization in One-Dimensional Randomly Disordered Optical Systems that are Periodic on Average, *Physical Review B*, vol. 47, pp. 13120–13125, 1993.
9. M. M. Sigalas and C. M. Soukoulis, Elastic-Wave Propagation through Disordered and/or Absorptive Layered Systems, *Physical Review B*, vol. 51, pp. 2780–2789, 1995
10. B. A. van Tiggelen, A. Lagendijk, and D. S. Wiersma, Reflection and Transmission of Waves near the Localization Threshold, *Physical Review Letters*, vol. 84, pp. 4333–4336, 2000.
11. S. H. Chang, H. Cao, and S. T. Ho, Cavity Formation and Light Propagation in Partially Ordered and Completely Random One-Dimensional Systems, *IEEE Journal of Quantum Electronics*, vol. 39, pp. 364–374, 2003.
12. V. Yannopapas, A. Modinos, and N. Stefanou, Anderson Localization of Light in Inverted Opals, *Physical Review B*, vol. 68, pp. 193205(1–4), 2003.
13. S. E. Skipetrov and B. A. van Tiggelen, Dynamics of Weakly Localized Waves, *Physical Review Letters*, vol. 92, pp. 113901(1–4), 2004.
14. A. R. McGurn, P. Sheng, and A. A. Maradudin, Strong Localization of Light in Two-Dimensional Disordered Dielectric Media, *Optical Communications*, vol. 91, pp. 175–179, 1992.
15. M. M. Sigalas, C. M. Soukoulis, C. T. Chan, and D. Turner, Localization of Electromagnetic Waves in Two-Dimensional Disordered Systems, *Physical Review B*, vol. 53, pp. 8340–8348, 1996.
16. M. Rusek and A. Orlowski, Anderson Localization of Electromagnetic Waves in Confined Dielectric Media, *Physical Review E*, vol. 59, pp. 3655–3660, 1999.
17. K. K. H. Wang and Z. Ye, Simulation Study of Localization of Electromagnetic Waves in Two-Dimensional Random Dipolar Systems, *Physical Review E*, vol. 68, pp. 066609(1–6), 2003.
18. Z. Ye and B. C. Gupta, About Wave Localization in Two-Dimensional Random Media, *Physics Letters A*, vol. 313, pp. 485–490, 2003.
19. M. Haney and R. Snieder, Breakdown of Wave Diffusion in 2D Due to Loops, *Physical Review Letters*, vol. 91, pp. 093902(1–4), 2003.
20. K. K. H. Wang and Z. Ye, Diffusive and Localization Behavior of Electromagnetic Waves in a Two-Dimensional Random Medium, *Physical Review E*, vol. 68, pp. 046608(1–10), 2003.
21. Y. A. Vlasov, M. A. Kaliteevski, and V. V. Nikolaev, Different Regimes of Light Localization in a Disordered Photonic Crystal, *Physical Review B*, vol. 60, pp. 1555–1562, 1999.
22. F. J. P. Schuurmans, M. Megens, D. Vanmaekelbergh, and A. Lagendijk, Light Scattering near the Localization Transition in Macroporous GaP Networks, *Physical Review Letters*, vol. 83, pp. 2183–2186, 1999.
23. A. A. Chabanov, M. Stoytcher, and A. Z. Genack, Statistical Signitures of Photon Localization, *Nature*, vol. 404, pp. 850–853, 2000.
24. A. A. Chabanov and A. Z. Genack, Photon Localization in Resonant Media, *Physical Review Letters*, vol. 87, pp. 153901(1–4), 2001.
25. D. S. Wiersma, M. P. Vanalbada, and A. Lagendijk, Random Laser, *Nature*, vol. 373, pp. 203–204, 1995.
26. H. Cao, Y. G. Zhao, S. T. Ho, E. W. Seelig, Q. H. Wang, and R. P. H. Chang, Random Laser Action in Semiconductor Powder, *Physical Review Letters*, vol. 82, pp. 2278–2281, 1999.
27. A. L. Burin, M. A. Ratner, H. Cao, and S. H. Chang, Random Laser in One Dimension, *Physical Review Letters*, vol. 88, pp. 093904(1–4), 2002.
28. H. Cao, J. Y. Y. Xu, Y. Ling, A. L. Burin, E. W. Seeling, X. Liu, and R. P. H. Chang, Random Lasers with Coherent Feedback, *IEEE Journal of Selected Topics in Quantum Electronics*, vol. 9, pp. 111–119, 2003.

29. G. van Soest, F. J. Poelwijk, and A. Lagendijk, Speckle Experiments in Random Lasers, *Physical Review E*, vol. 65, pp. 046603(1–5), 2002.
30. S. Mujumdar, S. Cavalieri, and D. S. Wiersma, Temperature-Tunable Random Lasing: Numerical Calculations and Experiments, *Journal of the Optical Society of America B-Optical Physics*, vol. 21, pp. 201–207, 2004.
31. M. A. Noginov, G. Zhu, A. A. Frantz, J. Novak, S. N. Williams, and I. Fowlkes, Dependence of $NdSc_3(BO_3)_4$ Random Laser Parameters on Particle Size, *Journal of the Optical Society of America B-Optical Physics*, vol. 21, pp. 191–200, 2004.
32. M. Patra, Theory of Photon Statistics of Random Lasers, *Physical Review A*, vol. 65, pp. 043809 (1–9), 2002.
33. Y. Feng, J. F. Bisson, J. R. Lu, S. H. Huang, K. Takaichi, A. Shirakawa, M. Musha, and K. Ueda, Thermal Effects in Quasi-Continuous-Wave Nd3+: Y3Al5O12 Nanocrystalline-Powder Random Laser, *Applied Physics Letters*, vol. 84, pp. 1040–1042, 2004.
34. S. M. Redmond, G. L. Armstrong, H. Y. Chan, E. Mattson, A. Mock, B. Li, R. Potts, M. Cui, S. C. Rand, S.L. Oliveira, J. Marchal, T. Hinklin, and R. M. Laine, Electrical Generation of Stationary Light in Random Scattering Media, *Journal of the Optical Society of America-B*, vol. 21, pp. 214–222, 2004.
35. M. Kaviany, Principles of Heat Transfer in Porous Media, Second Edition, Springer, New York, 1995.
36. J. C. Maxwell Garnett, Colours in Metal Glasses and in Metallic Films, Philosophical Transactions of the Royal Society of London, Series A, Containing Papers of a Mathematical or Physical Character, vol. 203, pp. 385–420, 1904.
37. O. Levy and D. Stroud, Maxwell Garnett Theory for Mixtures of Anisotropic Inclusions: Application to Conducting Polymers, *Physical Review B*, vol. 56, pp. 8035–8046, 1997.
38. Z. M. Zhang and M. I. Flik, Predicted Absorption of $YBa_2Cu_3O_7$/YSZ/Si Multilayer Structures for Infrared Detectors, *IEEE Transactions on Applied Superconductivity*, vol. 3, pp. 1604–1607, 1993.
39. Z. Knittl, Optics of Thin Films: An Optical Multilayer Theory, Wiley, New York, 1976.
40. S. Redmond, S. C. Rand, X. L. Ruan, and M. Kaviany, Multiple Scattering and Nonlinear Thermal Emission of Yb^{3+}, Er^{3+}: Y_2O_3 Nanopowders, *Journal of Applied Physics*, vol. 95, pp. 4069–4077, 2004.
41. E. Hecht, Optics, Addison Wesley, San Francisco, 2002.
42. Ansoft Corporation, High Frequency Structure Simulator (HFSS) software.
43. J. D. Kraus and D. A. Fleisch, Electromagnetics with Applications, McGraw-Hill, Boston, 1999.